DENOISING DIFFUSION GAMMA MODELS

Anonymous authors
Paper under double-blind review

ABSTRACT

Generative diffusion processes are an emerging and effective tool for image and speech generation. In the existing methods, the underlying noise distribution of the diffusion process is Gaussian noise. However, fitting distributions with more degrees of freedom could improve the performance of such generative models. In this work, we investigate other types of noise distribution for the diffusion process. Specifically, we introduce the Denoising Diffusion Gamma Model (DDGM) and show that noise from Gamma distribution provides improved results for image and speech generation. Our approach preserves the ability to efficiently sample state in the training diffusion process while using Gamma noise.

1 INTRODUCTION

Deep generative neural networks have shown significant progress over the last years. The main architectures for generation are: (i) VAE (Kingma & Welling, 2013) based, for example, NVAE (Vahdat & Kautz, 2020) and VQ-VAE (Razavi et al., 2019), (ii) GAN (Goodfellow et al., 2014) based, for example, StyleGAN (Karras et al., 2020) for vision application and WaveGAN (Donahue et al., 2018) for speech (iii) Flow-based, for example Glow (Kingma & Dhariwal, 2018) (iv) Autoregessive, for example, Wavenet for speech (Oord et al., 2016) and (v) Diffusion Probabilistic Models (Sohl-Dickstein et al., 2015), for example, Denoising Diffusion Probabilistic Models (DDPM) (Ho et al., 2020) and its implicit version DDIM (Song et al., 2020a).

Models from this last family have shown significant progress in generation capabilities in the last years, e.g., (Chen et al., 2020; Kong et al., 2020b), and have achieved results comparable to state-of-the-art generation architecture for both images and speech.

A DDPM is a Markov chain of latent variables. Two processes are modeled: (i) a diffusion process and (ii) a denoising process. During training, the diffusion process learns to transform data samples into Gaussian noise. Denoising is the reverse process and it is used during inference for generating data samples, starting from Gaussian noise. The second process can be conditioned on attributes to control the generation sample. To obtain high-quality synthesis, a large number of denoising steps is used (i.e. 1000 steps). A notable property of the diffusion process is a closed-form formulation of the noise that arises from accumulating diffusion stems. This allows sampling arbitrary states in the Markov chain of the diffusion process without calculating the previous steps.

In the Gaussian case, this property stems from the fact that adding Gaussian random variables leads to another Gaussian random variable. Other distributions have similar properties. For example, for the Gamma distribution, the sum of two random variables that share the scale parameter is a Gamma random variable of the same scale. The Poisson distribution has a similar property. However, its discrete nature makes it less suitable for DDPM.

In DDPM, the mean of the Gaussian random variables is set at zero. The Gamma random variable, with its two parameters (shape and scale), is better suited to fit the data than a Gaussian random variable with one degree of freedom (scale). Furthermore, the Gamma random variable generalizes other distributions, and many other distributions can be derived from it (Leemis & McQueston, 2008).

The added modeling capacity of the Gamma random variable can help speed up the convergence of the DDPM model. Consider, for example, a conventional DDPM model that was trained with Gaussian noise on the CelebA dataset (Liu et al., 2015).

The noise distribution throughout the diffusion process can be visualized by computing the histogram of the estimated residual noise in the generation process. The estimated residual noise $\hat{\epsilon}$ is given by

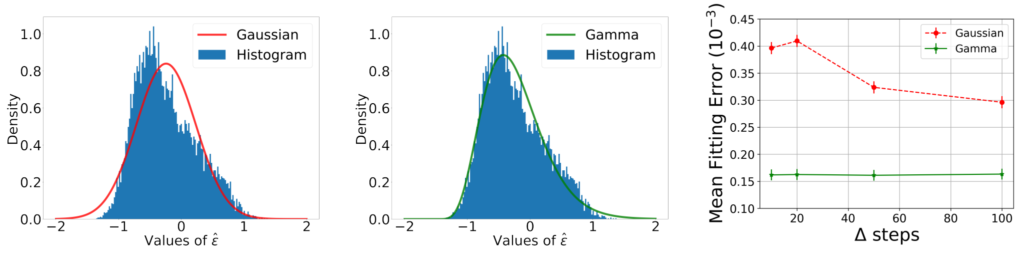

(a) (b) (c)

Figure 1: Fitting a distribution to the histogram of the generation error, which given by the scaled difference between x_0 and the image x_t after t DDPM steps $\hat{\epsilon} = \frac{\sqrt{\bar{\alpha}_t}x_0 - x_t}{\sqrt{1-|\bar{\alpha}_t|}}$. The model is a pretrained DDPM (Gaussian) celebA (64x64) model. (a) The fitting of a Gaussian to the histogram of a typical image after $t - 50$ steps. (b) Fitting a Gamma distribution. (c) The fitting error to Gaussian and Gamma distribution, measured as the MSE between the histogram and the fitted probability distribution function. Each point is the average value for the generation of 100 images. The vertical error bars denote the standard deviation.

$\hat{\epsilon} = \frac{\sqrt{\bar{\alpha}_t}x_0 - x_t}{\sqrt{1-|\bar{\alpha}_t|}}$, where $\bar{\alpha}_t$ is the noise schedule, x_0 is the data point and x_t is the estimate state at timestep t, as can be derived from Eq.4 from (Song et al., 2020a). Both a Gaussian distribution and Gamma distribution can then be fitted to this histogram, as shown in Fig. 1(a,b). As can be seen, the Gamma distribution provides a better fit to the estimated residual noise $\hat{\epsilon}$. Moreover, Fig. 1(c) presents the mean fitting error between the histogram and the fitted probability distribution function. Evidently, the Gamma distribution is a better fit than the Gaussian distribution. While the model was trained to estimate Gaussian noise, at inference time it has to address a different distribution.

In this paper, we investigate the non-Gaussian Gamma noise distribution. As noted, this distribution seems to fit the histogram of the generation error better than the Gaussian distribution, and it also has favorable properties such as its behavior under addition and scalar multiplication. The proposed models maintain the property of the diffusion process of sampling arbitrary states without calculating the previous steps. Our results are demonstrated in two major domains: vision and audio. In the first domain, the proposed method is shown to provide a better FID score for generated images. For speech data, we show that the proposed method improves various measures, such as Perceptual Evaluation of Speech Quality (PESQ) and short-time objective intelligibility (STOI).

2 Related Work

In their seminal work, Sohl-Dickstein et al. (2015) introduce the Diffusion Probabilistic Model. This model is applied to various domains, such as time series and images. The main drawback in the proposed model is that it needs up to thousands of iterative steps to generate a valid data sample. Song & Ermon (2019) proposed a diffusion generative model based on Langevin dynamics and the score matching method (Hyvärinen & Dayan, 2005). The model estimates the Stein score function (Liu et al., 2016) which is the gradient of the logarithm of data density. Given the Stein score function, the model can generate data points.

Denoising Diffusion Probabilistic Models (DDPM) (Ho et al., 2020) combine generative models based on score matching and neural Diffusion Probabilistic Models into a single model. Similarly, in Chen et al. (2020); Kong et al. (2020a) a generative neural diffusion process based on score matching was applied to speech generation. These models achieve state-of-the-art results for speech generation, and show superior results over well-established methods, such as Wavernn (Kalchbrenner et al., 2018), Wavenet (Oord et al., 2016), and GAN-TTS (Bińkowski et al., 2019).

Diffusion Implicit Models (DDIM) offer a way to accelerate the denoising process (Song et al., 2020a). The model employs a non-Markovian diffusion process to generate a higher quality sample. The model helps reduce the number of diffusion steps, e.g., from a thousand steps to a few hundred.

Algorithm 1 DDPM training procedure.

```
Input: dataset $d$, diffusion process length $T$, noise schedule $\beta_1, ..., \beta_T$
repeat
    $x_0 \sim d(x_0)$
    $t \sim \mathcal{U}(\{1, ..., T\})$
    $\varepsilon \sim \mathcal{N}(0, I)$
    $x_t = \sqrt{\bar{\alpha}_t} x_0 + \sqrt{1 - \bar{\alpha}_t} \varepsilon$
    Take gradient descent step on:
    $\|\varepsilon - \varepsilon_\theta(x_t, t)\|_1$
until converged
```

Algorithm 2 DDPM sampling algorithm

```
$x_T \sim \mathcal{N}(0, I)$
for t= T, ..., 1 do
    $z \sim \mathcal{N}(0, I)$
    $\hat{\varepsilon} = \varepsilon_\theta(x_t, t)$
    $x_{t-1} = \frac{x_t - \frac{1-\alpha_t}{\sqrt{1-\bar{\alpha}_t}} \hat{\varepsilon}}{\sqrt{\alpha_t}}$
    if $t \neq 1$ then
        $x_{t-1} = x_{t-1} + \sigma_t z$
    end if
end for
return $x_0$
```

Dhariwal & Nichol (2021) find a better diffusion architecture through a series of exploratory experiments, leading to the Ablated Diffusion Model (ADM). This model outperforms the state-of-the-art in image synthesis, which was previously provided by GAN based-models, such as BigGAN-deep (Brock et al., 2018) and StyleGAN2 (Karras et al., 2020). ADM is further improved using a novel Cascaded Diffusion Model (CDM). Our contribution is fundamental and can be incorporated into the proposed ADM and CDM architectures.

Watson et al. (2021) proposed an efficient method for sampling from diffusion probabilistic models by a dynamic programming algorithm that finds the optimal discrete time schedules. Choi et al. (2021) introduces the Iterative Latent Variable Refinement (ILVR) method for guiding the generative process in DDPM. Moreover, Kong & Ping (2021) systematically investigates fast sampling methods for diffusion denoising models. Lam et al. (2021) propose bilateral denoising diffusion models (BDDM), which take significantly fewer steps to generate high-quality samples.

Huang et al. (2021) derive a variational framework for likelihood estimating of the marginal likelihood of continuous-time diffusion models. Moreover, Kingma et al. (2021) shows equivalence between various diffusion processes by using a simplification of the variational lower bound (VLB).

Song et al. (2020b) show that score-based generative models can be considered a solution to a stochastic differential equation. Gao et al. (2020) provide an alternative approach for training an energy-based generative model using a diffusion process.

Another line of work in audio is that of neural vocoders based on a denoising diffusion process. WaveGrad (Chen et al., 2020) and DiffWave (Kong et al., 2020a) are conditioned on the mel-spectrogram and produce high-fidelity audio samples, using as few as six steps of the diffusion process. These models outperform adversarial non-autoregressive baselines. Popov et al. (2021) propose a text-to-speech diffusion base model, which allows generating speech with the flexibility of controlling the trade-off between sound quality and inference speed.

Diffusion models were also applied to natural language processing tasks. Hoogeboom et al. (2021) proposed a multinomial diffusion process for categorical data and applied it to language modeling. Austin et al. (2021) generalize the multinomial diffusion process with Discrete Denoising Diffusion Probabilistic Models (D3PMs) and improve the generated results for the text8 and One Billion Word (LM1B) datasets.

3 Diffusion models for Gamma Distribution

We start by recapitulating the Gaussian case, after which we derive diffusion models for the Gamma distribution.

3.1 Background - Gaussian DDPM

Diffusion networks learn the gradients of the data log density:

$$s(y) = \nabla_y \log p(y) \tag{1}$$

By using Langevin Dynamics and the gradients of the data log density $\nabla_y \log p(y)$, a sample procedure from the probability can be done by:

$$\tilde{y}_{i+1} = \tilde{y}_i + \frac{\eta}{2} s(\tilde{y}_i) + \sqrt{\eta} z_i \tag{2}$$

where $z_i \sim \mathcal{N}(0, I)$ and $\eta > 0$ is the step size.

The diffusion process in DDPM (Ho et al., 2020) is defined by a Markov chain that gradually adds Gaussian noise to the data according to a noise schedule. The diffusion process is defined by:

$$q(x_{1:T}|x_0) = \prod_{t=1}^{T} q(x_t|x_{t-1}) \,, \tag{3}$$

where T is the length of the diffusion process, and $x_T, ..., x_t, x_{t-1}, ..., x_0$ is a sequence of latent variables with the same size as the clean sample x_0. The Diffusion process is parameterized with a set of parameters called noise schedule ($\beta_1, \ldots \beta_T$), which defines the variance of the noise added at each step:

$$q(x_t|x_{t-1}) := \mathcal{N}(x_t; \sqrt{1-\beta_t} x_{t-1}, \beta_t \mathbf{I}) \,, \tag{4}$$

Since we are using a Gaussian noise random variable at each step, the diffusion process can be simulated for any number of steps with the closed formula:

$$x_t = \sqrt{\bar{\alpha}_t} x_0 + \sqrt{1-\bar{\alpha}_t} \varepsilon \,, \tag{5}$$

where $\alpha_i = 1 - \beta_i$, $\bar{\alpha}_t = \prod_{i=1}^{t} \alpha_i$ and $\varepsilon = \mathcal{N}(0, \mathbf{I})$.

Diffusion models are a class of generative neural network of the form $p_\theta(x_0) = \int p_\theta(x_{0:T}) dx_{0:T}$ that learn to reverse the diffusion process. One can write that:

$$p_\theta(x_{0:T}) = p(x_T) \prod_{t=1}^{T} p_\theta(x_{t-1}|x_t) \tag{6}$$

As described in (Ho et al., 2020), one can learn to predict the noise present in the data with a network ε_θ and sample from $p_\theta(x_{t-1}|x_t)$ using the following formula:

$$x_{t-1} = \frac{x_t - \frac{1-\alpha_t}{\sqrt{1-\bar{\alpha}_t}} \varepsilon_\theta(x_t, t)}{\sqrt{\bar{\alpha}_t}} + \sigma_t \varepsilon \,, \tag{7}$$

where ε is white noise and σ_t is the standard deviation of added noise. (Song et al., 2020a) use ${\sigma_t}^2 = \beta_t$.

The training procedure of ε_θ is defined in Alg.1. Given the input dataset d, the algorithm samples ϵ, x_0 and t. The noisy latent state x_t is calculated and fed to the DDPM neural network ε_θ. A gradient descent step is taken in order to estimate the ε noise with the DDPM network ε_θ. The objective for the diffusion model is a variational bound on the model data log likelihood.

The complete inference algorithm present at Alg. 2. Starting from Gaussian noise and then reversing the diffusion process step-by-step, by iteratively employing the update rule of Eq. 7. To perform generation with few denoising iterations one can use the update equation introduced in Song et al. (2020a). This work greatly improves the results of diffusion networks when performing sampling with few generative steps.

$$x_{n-1} = \sqrt{\bar{\alpha}_{n-1}} \hat{x}_{0,n} + \sqrt{1 - \bar{\alpha}_{n-1} - \tilde{\sigma}_n^2} \varepsilon_\theta(x_n, \bar{\alpha}_n) + \tilde{\sigma}_n \varepsilon \,, \tag{8}$$

Intuitively this equation changes the added noise for the generative steps. It uses a blend of the noise from the previous state ($\varepsilon_\theta(x_n, \bar{\alpha}_n)$ and random noise (ε). One can write $\tilde{\sigma} = \eta \sqrt{\beta_n (1 - \bar{\alpha}_{n-1})(1 - \bar{\alpha}_n)}$ this allows to have a simple parameter η to choose the ratio of the blend. On top of improving the results in short samplings regimes, this allows to generate in a deterministic way when using $\eta = 0$.

3.2 Denoising Diffusion Gamma Models (DDGM)

We expand the framework of diffusion generative processes by incorporating a new noise distribution, namely the Gamma Distribution. We call this new type of models Denoising Diffusion Gamma Models. First, we define the Gamma diffusion process, then we present a way to sample from this process, and finally we show how to train those models by computing the variational lower bound and deriving a novel loss function from it.

3.2.1 The Gamma Model

In the Gaussian case the diffusion equation (Eq. 4) can be written as:

$$x_t = \sqrt{1-\beta_t} x_{t-1} + \sqrt{\beta_t}\epsilon_t \tag{9}$$

where ϵ_t is the Gaussian noise of step t. One can denote $\Gamma(k,\theta)$ as the Gamma distribution, where k and θ are the shape and the scale respectively. We modify Eq. 9 by adding, during the diffusion process, noise that follows a Gamma distribution:

$$x_t = \sqrt{1-\beta_t} x_{t-1} + (g_t - \mathbb{E}(g_t)) \tag{10}$$

where $g_t \sim \Gamma(k_t, \theta_t)$, $\theta_t = \sqrt{\bar{\alpha}_t}\theta_0$ and $k_t = \dfrac{\beta_t}{\alpha_t {\theta_0}^2}$. Note that θ_0 and β_t are hyperparameters (and the noise term has zero mean.)

Since the sum of Gamma random variables (with the same scale parameter) is distributed as Gamma distribution, one can derive a closed form for x_t, i.e. an equation to calculate x_t from x_0:

$$x_t = \sqrt{\bar{\alpha}_t} x_0 + (\bar{g}_t - \bar{k}_t\theta_t) \tag{11}$$

where $\bar{g}_t \sim \Gamma(\bar{k}_t, \theta_t)$ and $\bar{k}_t = \sum_{i=1}^{t} k_i$.

Lemma 1. *Let $\theta_0 \in \mathbb{R}$, Assuming $\forall t \in \{1, ..., T\}$, $k_t = \dfrac{\beta_t}{\alpha_t {\theta_0}^2}$, $\theta_t = \sqrt{\bar{\alpha}_t}\theta_0$, and $g_t \sim \Gamma(k_t, \theta_t)$. Then $\forall t \in \{1, ..., T\}$ the following hold:*

$$E(g_t - E(g_t)) = 0, V(g_t - E(g_t)) = \beta_t \tag{12}$$

$$x_t = \sqrt{\bar{\alpha}_t} x_0 + (\bar{g}_t - E(\bar{g}_t)) \tag{13}$$

where $\bar{g}_t \sim \Gamma(\bar{k}_t, \theta_t)$ and $\bar{k}_t = \sum_{i=1}^{t} k_i$

The complete proof for Lemma 1 is given in Appendix A.1.

Similarly to Eq.7, the inference is given by:

$$x_{t-1} = \frac{x_t - \frac{1-\alpha_t}{\sqrt{1-\bar{\alpha}_t}}\varepsilon_\theta(x_t, t)}{\sqrt{\alpha_t}} + \sigma_t \frac{\bar{g}_t - E(\bar{g}_t)}{\sqrt{V(\bar{g}_t)}} \tag{14}$$

In Algorithm 3 we describe the training procedure. As input we have the: (i) initial scale θ_0, (ii) the dataset d, (iii) the maximum number of steps in the diffusion process T and (iv) the noise schedule $\beta_1, ..., \beta_T$. The training algorithm sample: (i) an example x_0, (ii) number of step t and (iii) noise ε. Then it calculates x_t from x_0 by using Eq.11. The neural network ε_θ has an input x_t and is conditional on the time step t. Next, it takes a gradient descent step to approximate the normalized noise $\frac{\bar{g}_t - \bar{k}_t\theta_t}{\sqrt{1-|\bar{\alpha}_t|}}$ with the neural network ε_θ. The main changes between Algorithm 3 and the single Gaussian case (i.e. Alg. 1) are the following: (i) calculating the Gamma parameters, (ii) x_t update equation and (iii) the gradient update equation.

The inference procedure is given in Algorithm 4. It starts from a zero mean noise x_T sampled from $\Gamma(\theta_T, \bar{k}_T)$. Next, for T steps the algorithm estimates x_{t-1} from x_t by using Eq.14. Note that as in (Song et al., 2020a) $\sigma_t = \beta_t$. Algorithm 4 replaces the Gaussian version (i.e. Alg. 2) with the following: (i) the starting sampling point x_T, (ii) the sampling noise z and (iii) the x_t update equation.

Algorithm 3 Gamma Training Algorithm

```
Input: initial scale $\theta_0$, dataset $d$, diffusion process length $T$, noise schedule $\beta_1, ..., \beta_T$
repeat
    $x_0 \sim d(x_0)$
    $t \sim \mathcal{U}(\{1, ..., T\})$
    $\bar{g}_t \sim \Gamma(\bar{k}_t, \theta_t)$
    $x_t = \sqrt{\bar{\alpha}_t} x_0 + (\bar{g}_t - \bar{k}_t \theta_t)$
    Take a gradient descent step on:
    $\left| \frac{\bar{g}_t - \bar{k}_t \theta_t}{\sqrt{1 - |\bar{\alpha}_t|}} - \varepsilon_\theta(x_t, t) \right|$
until converged
```

Algorithm 4 Gamma Inference Algorithm

```
$\gamma \sim \Gamma(\theta_T, \bar{k}_T)$
$x_T = \gamma - \theta_T * \bar{k}_T$
for t = T, ..., 1 do
    $x_{t-1} = \frac{x_t - \frac{1-\alpha_t}{\sqrt{1-\bar{\alpha}_t}} \epsilon(x_t, t)}{\sqrt{\alpha_t}}$
    if t > 1 then
        $z \sim \Gamma(\theta_{t-1}, \bar{k}_{t-1})$
        $z = \frac{z - \theta_{t-1} \bar{k}_{t-1}}{\sqrt{(1 - \bar{\alpha}_t)}}$
        $x_{t-1} = x_{t-1} + \sigma_t z$
    end if
end for
```

3.2.2 The Reverse Process for DDGM

The reverse process $q(x_{t-1}|x_0, x_t)$ defines the underlying generation process. Therefore, in this section, we will obtain the reverse process for the Gamma denoising diffusion model. Furthermore, we will use the reverse process $q(x_{t-1}|x_0, x_t)$ to obtain the variational lower bound and the appropriate loss function for the Gamma distribution denoising diffusion model.

Lemma 2. *Denote $q(x_{t-1}|x_0, x_t)$ as the reverse process of the proposed Gamma diffusion model. Then, the reverse process is proportional to:*

$$q(x_{t-1}|x_0, x_t) \propto \frac{X_t^{k_t - 1} e^{-X_t/\theta_t} \bar{X}_{t-1}^{\bar{k}_{t-1} - 1} e^{-\bar{X}_{t-1}/\theta_{t-1}}}{\bar{X}_t^{\bar{k}_t - 1} e^{-\bar{X}_t/\theta_t}} \tag{15}$$

where

1. $X_t = x_t - \sqrt{1 - \beta_t} x_{t-1} + k_t \theta_t$
2. $\bar{X}_t = x_t - \sqrt{\bar{\alpha}_t} x_0 + \bar{k}_t \theta_t$
3. $\bar{X}_{t-1} = x_{t-1} - \sqrt{\bar{\alpha}_{t-1}} x_0 + \bar{k}_{t-1} \theta_{t-1}$

The complete proof for Lemma 2 is given in Appendix A.1. It states that the reverse process is proportional to three Gamma random variables X_t, $\bar{X}_{t-1}$, and $\bar{X}_t$. This observation allows us to develop the associated variational lower bound.

3.2.3 Variational Lower Bound for DDGM

Denoising diffusion models (Ho et al., 2020) trained by optimizing the usual variational bound on negative log likelihood:

$$E\left[-log(p_\theta(x_0)\right] \leq E_q\left[-\log p(x_T) - \sum_{t \geq 1} \log \frac{p_\theta(x_{t-1}|x_t)}{q(x_t|x_{t-1})} \right] = L_{VLB} \tag{16}$$

To get the variational lower bound for the proposed Gamma denoising diffusion model, one can use Eq.5 from Ho et al. (2020):

$$L_{VLB} = E_q\left[L_T + \sum_{t>1} L_{t-1} + L_0 \right] \tag{17}$$

where L_T, L_{t-1} and L_0 define by:

1. $L_T = D_{KL}(q(x_T|x_0)||q(x_T))$
2. $L_{t-1} = D_{KL}(q(x_{t-1}|x_0, x_t)||p_\theta(x_{t-1}|\hat{x}_0, x_t))$
3. $L_0 = -\log(p_\theta(x_0|x_1))$

It should be noted that in the Gaussian case the KL terms have a closed form. L_T is constant and ignored during training since it doesn't have learnable parameters. Moreover, in (Ho et al., 2020) L_0 modeled with discrete decoder, however, in our proposed model we empirically found that the impact L_0 is negligible and can be removed.

Therefore, to calculate the variatonal lower bound one needs to obtain:

$$L_{t-1} = D_{KL}(q(x_{t-1}|x_0, x_t)||p_\theta(x_{t-1}|\hat{x}_0, x_t)) \tag{18}$$

where:

$$\hat{x}_0 = \frac{x_t - \sqrt{1-\bar{\alpha}_t}\varepsilon_\theta(x_t, t)}{\sqrt{\bar{\alpha}_t}} \tag{19}$$

Lemma 3. *The L_{t-1} for the proposed Gamma diffusion model is upper bounded by the following L_1 norm:*

$$L_{t-1} \leq \left(C_1 + C_2 + \frac{C_3}{\bar{g}_t} + \frac{C_4}{\bar{g}_{t-1}}\right)|x_0 - \hat{x}_0| \tag{20}$$

where C_1, C_2, C_3 and C_4 are constant terms.

The complete proof for Lemma 3 is given in Appendix A.1.

As can be seen, the variational lower bound is bounded by some constant forms multiplied by the L1 norm between the data point x_0 and its estimation $\hat{x}_0$. The constant terms C_1, C_2, C_3 and C_4 as well as $\bar{g}_t$ and $\bar{g}_{t-1}$ are known values during the training.

3.2.4 Loss Function for DDGM

Denoising diffusion probabilistic models use the variational lower bound to minimize the negative log likelihood. As described in Sec.3.2.1, one can minimize the variational lower bound by L_t for $t \geq 1$. To do so, one can minimize the L1 norm from Eq.34. Our model optimizes the L1 norm between the sampled noise ϵ_θ and the estimated noise ε_θ. This is verified in the following lemmas.

Lemma 4. *Minimizing the variational lower bound for DDGM (i.e. L_t for $t \geq 1$) is equivalent to minimizing the L1 norm between the sampled noise and the estimated noise:*

$$\mathcal{L} = \left|\frac{\bar{g}_t - \bar{k}_t\theta_t}{\sqrt{1-\bar{\alpha}_t}} - \varepsilon_\theta(x_t, t)\right| \tag{21}$$

The complete proof for Lemma 4 is given in Sec.A.4 at the appendix. Thus, the loss that is used in the Alg.3 is given by $\mathcal{L} = \left|\frac{\bar{g}_t - \bar{k}_t\theta_t}{\sqrt{1-\bar{\alpha}_t}} - \varepsilon_\theta(x_t, t)\right|$.

4 Experiments

4.1 Speech Generation

For our speech experiments we used a version of Wavegrad (Chen et al., 2020) based on this implementation Vovk (2020) (under BSD-3-Clause License). We evaluate our model with high-level perceptual quality of speech measurements, PESQ (Rix et al., 2001) and STOI (Taal et al., 2011). We used the standard Wavegrad method with the Gaussian diffusion process as a baseline. We use two Nvidia Volta V100 GPUs to train our models.

For all the experiments, the inference noise schedules $(\beta_0, .., \beta_T)$ were defined as described in the Wavegrad paper (Chen et al., 2020). For 1000 and 100 iterations the noise schedule is linear, for 25 iterations it comes from the Fibonacci and for 6 iterations we performed a model-dependent grid search to find the best noise schedule parameters. For other hyper-parameters (e.g. learning rate, batch size, etc) we use the same as in Wavegrad (Chen et al., 2020). Training was performed using the following form of Eq. 10, e.g. $\theta_t = \sqrt{\bar{\alpha}_t}\theta_0$ and $k_t = \frac{\beta_t}{\bar{\alpha}_t{\theta_0}^2}$. Our best results were obtained using $\theta_0 = 0.001$.

Table 1: PESQ and STOI metrics for the LJ dataset for various Wavegrad-like models.

	PESQ (↑)				STOI (↑)			
Model \ Iteration	6	25	100	1000	6	25	100	1000
WaveGrad (Chen et al., 2020)	2.78	3.194	3.211	3.290	0.924	0.957	0.958	0.959
DDGM (ours)	**3.07**	**3.208**	**3.214**	**3.308**	**0.948**	**0.972**	**0.969**	**0.969**

Table 2: FID (↓) score comparison for CelebA(64x64) dataset. Lower is better.

Model \ Iteration	10	20	50	100	1000
DDPM (Ho et al., 2020)	299.71	183.83	71.71	45.2	**3.26**
DDGM - Gamma Distribution DDPM (ours)	**35.59**	**28.24**	**20.24**	**14.22**	4.09
DDIM (Song et al., 2020a)	17.33	13.73	9.17	6.53	3.51
DDGM - Gamma Distribution DDIM (ours)	**11.64**	**6.83**	**4.28**	**3.17**	**2.92**

Table 3: FID (↓) score comparison for LSUN Church (256x256) dataset. Lower is better. The results of DDIM for $T = 1000$ are not reported by Song et al. (2020a).

Model \ Iteration	10	20	50	100	1000
DDPM (Ho et al., 2020)	51.56	23.37	11.16	8.27	7.89
DDGM - Gamma Distribution DDPM (ours)	**28.56**	**19.68**	**10.53**	**7.87**	**6.91**
DDIM (Song et al., 2020a)	19.45	12.47	10.84	10.58	NA
DDGM - Gamma Distribution DDIM (ours)	**18.11**	**11.32**	**10.31**	**8.75**	**7.34**

Table 4: FID (↓) score comparison for ImageNet (64x64) dataset. Lower is better.

Model \ Iteration	10	20	50	100	1000
DDIM (Song et al., 2020a)	42.88	35.40	31.98	30.74	28.81
DDGM - Gamma Distribution DDIM (ours)	**42.17**	**31.84**	**28.75**	**27.02**	**24.22**

Table 5: FID (↓) score comparison during the inference process for CelebA (64x64) dataset for the full inference procedure and for an earlier stage in the process.

Iteration	T=10	T=20	T=100
Model	(first 5 steps/10 steps)	(first 10 steps/20 steps)	(first 50 steps/100 steps)
DDIM (Song et al., 2020a)	54.32/17.33	43.35/13.73	36.68/6.53
DDGM (ours)	55.40/11.64	42.43/6.83	35.20/3.17

Results Tab. 1 presents the PESQ and STOI measurement for the LJ dataset (Ito & Johnson, 2017). As can be seen, for the proposed Gamma denoising diffusion model our results are better than the Wavegrad baseline for all number of iterations in both PESQ and STOI.

4.2 Image Generation

Our model is based on the DDIM implementation available in (Jiaming Song & Ermon, 2020) (under the MIT license). We trained our model on three image datasets (i) CelebA 64x64 (Liu et al., 2015), (ii) LSUN Church 256x256 (Yu et al., 2015) and (iii) ImageNet 64x64 (Deng et al., 2009). The Fréchet Inception Distance (FID) (Heusel et al., 2017) is used as the benchmark metric. For all experiments, similarly to previous work (Song et al., 2020a), we compute the FID score with $50,000$ generated images, using the torch-fidelity implementation (Obukhov et al., 2020). Similar to (Song et al., 2020a), the training noise schedule $\beta_1, ..., \beta_T$ is linear with values raging from 0.0001 to 0.02. For other hyperparameters (e.g. learning rate, batch size etc) we use the same parameters that appear in DDPM (Ho et al., 2020). We use eight Nvidia Volta V100 GPUs to train our models. The θ_0 parameter for Gamma distribution set to 0.001.

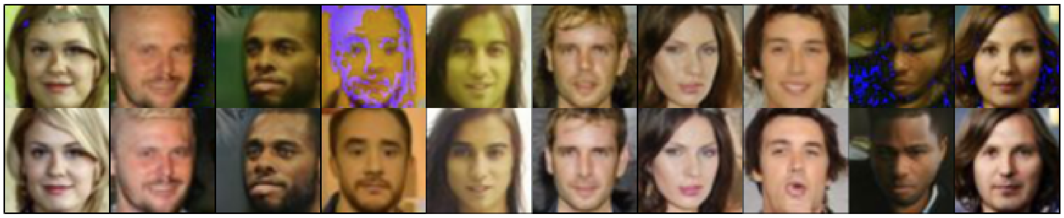

Figure 2: Typical examples of images generated with 100 iterations and $\eta = 0$. For models trained with different noise distributions - (i) First row - Gaussian noise and (ii) Second row - Gamma noise. All models start from the same noise instance.

Results We test our models with the inference procedure from DDPM (Ho et al., 2020) and DDIM (Song et al., 2020a). In Tab. 2 we provide the FID score for CelebA (64x64) dataset (Liu et al., 2015) (under non-commercial research purposes license). As can be seen for DDPM inference procedure for $10, 20, 50, 100$ steps, the best results were obtained from the Gamma model, which improves results by a gap of 264 FID scores for ten iterations. For 100 iterations, the Gamma model improves results by 31 FID scores. For 1000 iterations, the best results were obtained from the DDPM model. Nevertheless, our Gamma model obtains results that are closer to the DDPM by a gap of 0.83. For the DDIM procedure, the best results were obtained with the Gamma model for all number of iterations. Fig. 2 presents samples generated by the three models. Our models provide better quality images when compared to DDPM and DDIM methods.

In Tab. 3 we provide the FID score for the LSUN church dataset (Yu et al., 2015). As can be seen, the Gamma model improves results over the baseline for $10, 20, 50, 100, 1000$ iterations.

Tab. 4 lists the FID score for the ImageNet 64x64 dataset. The Gamma model obtains better results than the DDIM baseline method for all iteration counts. Figure 3 compares between our proposed DDGM and the baseline DDIM method. The random samples are generated with 1000 iterations with the DDIM generation algorithm and $\eta = 0$. In each of the nine instances, the same random noise is used as x_{1000} for both models.

In Tab. 5, we present results for training the network on a Markov chain of size T and perform all the processes until step $T/2$, from which we infer x_0 in one inference step. As can be seen, after the $T/2$ first iterations, there is no significant difference between Gaussian and Gamma networks. However, after the remaining $T/2$ iterations, the Gamma based model obtains a performance GAP over the Gaussian model. This suggests that our method is improving the results mostly during the final stage of the inference process.

5 Conclusions

We present a novel Gamma diffusion model. The model employs a Gamma noise distribution. A key enabler for using these distributions is a closed-form formulation (Eq. 11) of the multi-step noising process, which allows for efficient training. We also present the reverse process and the variational lower bound for the Gamma diffusion model. The proposed model improves the quality of generated image and audio, as well as the speed of generation in comparison to conventional, Gaussian-based diffusion processes. Our DDGM methods shows that diffusion model can benefit from non-Gaussian noise distributions. This comes at a cost of adding one new hyperparameter to tune (θ_0). Working with other probability distributions, such as mixture models, may improve results even further.

Reproducibility Statement

We provide in the supplementary file the complete code that was used to perform all of our experiments. This archive includes audio samples and the code for both image and speech experiments. Hyperparameters choices are clearly stated in Sec. 4 and the values are obtained from publicly available implementation of previous work. The proof of all the theoretical results are available in the appendix or are derived in the paper.

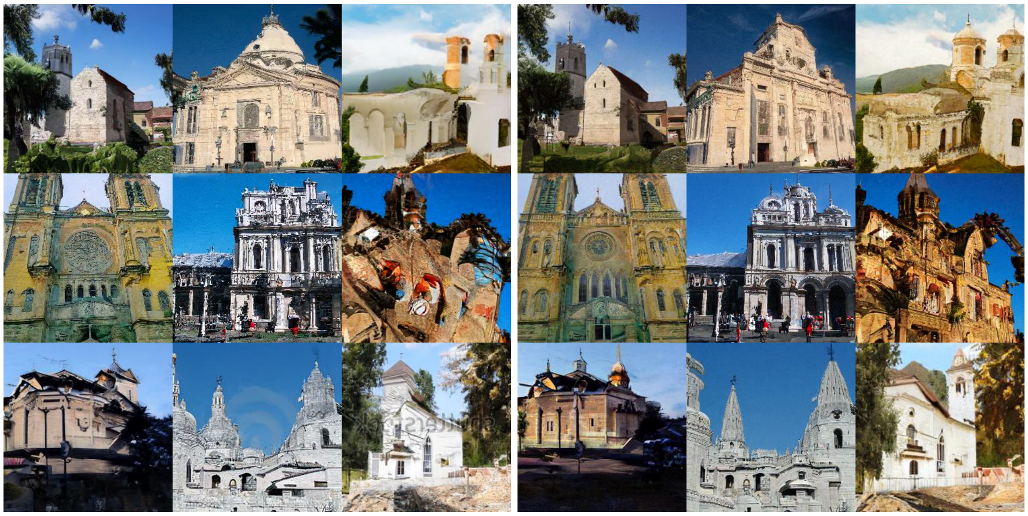

Figure 3: Comparison of generated samples with the (left) Gaussian noise (DDIM) and (right) Gamma noise (DDGM). In each of the nine cases, the two models start from the same noise instance, which leads to similar output images between the models.

REFERENCES

Jacob Austin, Daniel Johnson, Jonathan Ho, Danny Tarlow, and Rianne van den Berg. Structured denoising diffusion models in discrete state-spaces. *arXiv preprint arXiv:2107.03006*, 2021.

Mikołaj Bińkowski, Jeff Donahue, Sander Dieleman, Aidan Clark, Erich Elsen, Norman Casagrande, Luis C Cobo, and Karen Simonyan. High fidelity speech synthesis with adversarial networks. *arXiv preprint arXiv:1909.11646*, 2019.

Andrew Brock, Jeff Donahue, and Karen Simonyan. Large scale gan training for high fidelity natural image synthesis. *arXiv preprint arXiv:1809.11096*, 2018.

Nanxin Chen, Yu Zhang, Heiga Zen, Ron J Weiss, Mohammad Norouzi, and William Chan. Wavegrad: Estimating gradients for waveform generation. *arXiv preprint arXiv:2009.00713*, 2020.

Jooyoung Choi, Sungwon Kim, Yonghyun Jeong, Youngjune Gwon, and Sungroh Yoon. Ilvr: Conditioning method for denoising diffusion probabilistic models. *arXiv preprint arXiv:2108.02938*, 2021.

Jia Deng, Wei Dong, Richard Socher, Li-Jia Li, Kai Li, and Li Fei-Fei. Imagenet: A large-scale hierarchical image database. In *2009 IEEE conference on computer vision and pattern recognition*, pp. 248–255. Ieee, 2009.

Prafulla Dhariwal and Alex Nichol. Diffusion models beat gans on image synthesis. *arXiv preprint arXiv:2105.05233*, 2021.

Chris Donahue, Julian McAuley, and Miller Puckette. Adversarial audio synthesis. *arXiv preprint arXiv:1802.04208*, 2018.

Ruiqi Gao, Yang Song, Ben Poole, Ying Nian Wu, and Diederik P Kingma. Learning energy-based models by diffusion recovery likelihood. *arXiv preprint arXiv:2012.08125*, 2020.

Ian J Goodfellow, Jean Pouget-Abadie, Mehdi Mirza, Bing Xu, David Warde-Farley, Sherjil Ozair, Aaron Courville, and Yoshua Bengio. Generative adversarial networks. *arXiv preprint arXiv:1406.2661*, 2014.

Martin Heusel, Hubert Ramsauer, Thomas Unterthiner, Bernhard Nessler, and Sepp Hochreiter. Gans trained by a two time-scale update rule converge to a local nash equilibrium. *arXiv preprint arXiv:1706.08500*, 2017.

Jonathan Ho, Ajay Jain, and Pieter Abbeel. Denoising diffusion probabilistic models. *arXiv preprint arXiv:2006.11239*, 2020.

Emiel Hoogeboom, Didrik Nielsen, Priyank Jaini, Patrick Forré, and Max Welling. Argmax flows and multinomial diffusion: Towards non-autoregressive language models. *arXiv preprint arXiv:2102.05379*, 2021.

Chin-Wei Huang, Jae Hyun Lim, and Aaron Courville. A variational perspective on diffusion-based generative models and score matching. *arXiv preprint arXiv:2106.02808*, 2021.

Aapo Hyvärinen and Peter Dayan. Estimation of non-normalized statistical models by score matching. *Journal of Machine Learning Research*, 6(4), 2005.

Keith Ito and Linda Johnson. The lj speech dataset. `https://keithito.com/LJ-Speech-Dataset/`, 2017.

Chenlin Meng Jiaming Song and Stefano Ermon. Denoising diffusion implicit models. `https://github.com/ermongroup/ddim`, 2020.

Nal Kalchbrenner, Erich Elsen, Karen Simonyan, Seb Noury, Norman Casagrande, Edward Lockhart, Florian Stimberg, Aaron Oord, Sander Dieleman, and Koray Kavukcuoglu. Efficient neural audio synthesis. In *International Conference on Machine Learning*, pp. 2410–2419. PMLR, 2018.

Tero Karras, Samuli Laine, Miika Aittala, Janne Hellsten, Jaakko Lehtinen, and Timo Aila. Analyzing and improving the image quality of stylegan. In *Proceedings of the IEEE/CVF Conference on Computer Vision and Pattern Recognition*, pp. 8110–8119, 2020.

Diederik P Kingma and Prafulla Dhariwal. Glow: Generative flow with invertible 1x1 convolutions. *arXiv preprint arXiv:1807.03039*, 2018.

Diederik P Kingma and Max Welling. Auto-encoding variational bayes. *arXiv preprint arXiv:1312.6114*, 2013.

Diederik P Kingma, Tim Salimans, Ben Poole, and Jonathan Ho. Variational diffusion models. *arXiv preprint arXiv:2107.00630*, 2021.

Zhifeng Kong and Wei Ping. On fast sampling of diffusion probabilistic models. *arXiv preprint arXiv:2106.00132*, 2021.

Zhifeng Kong, Wei Ping, Jiaji Huang, Kexin Zhao, and Bryan Catanzaro. Diffwave: A versatile diffusion model for audio synthesis. *arXiv preprint arXiv:2009.09761*, 2020a.

Zhifeng Kong, Wei Ping, Jiaji Huang, Kexin Zhao, and Bryan Catanzaro. Diffwave: A versatile diffusion model for audio synthesis. *arXiv preprint arXiv:2009.09761*, 2020b.

Max WY Lam, Jun Wang, Rongjie Huang, Dan Su, and Dong Yu. Bilateral denoising diffusion models. *arXiv preprint arXiv:2108.11514*, 2021.

Lawrence M Leemis and Jacquelyn T McQueston. Univariate distribution relationships. *The American Statistician*, 62(1):45–53, 2008.

Qiang Liu, Jason Lee, and Michael Jordan. A kernelized stein discrepancy for goodness-of-fit tests. In *International conference on machine learning*, pp. 276–284. PMLR, 2016.

Ziwei Liu, Ping Luo, Xiaogang Wang, and Xiaoou Tang. Deep learning face attributes in the wild. In *Proceedings of International Conference on Computer Vision (ICCV)*, December 2015.

Anton Obukhov, Maximilian Seitzer, Po-Wei Wu, Semen Zhydenko, Jonathan Kyl, and Elvis Yu-Jing Lin. High-fidelity performance metrics for generative models in pytorch, 2020. URL `https://github.com/toshas/torch-fidelity`. Version: 0.2.0, DOI: 10.5281/zenodo.3786540.

Aaron van den Oord, Sander Dieleman, Heiga Zen, Karen Simonyan, Oriol Vinyals, Alex Graves, Nal Kalchbrenner, Andrew Senior, and Koray Kavukcuoglu. Wavenet: A generative model for raw audio. *arXiv preprint arXiv:1609.03499*, 2016.

Vadim Popov, Ivan Vovk, Vladimir Gogoryan, Tasnima Sadekova, and Mikhail Kudinov. Grad-tts: A diffusion probabilistic model for text-to-speech. *arXiv preprint arXiv:2105.06337*, 2021.

Ali Razavi, Aaron van den Oord, and Oriol Vinyals. Generating diverse high-fidelity images with vq-vae-2. *arXiv preprint arXiv:1906.00446*, 2019.

A. W. Rix, J. G. Beerends, M. P. Hollier, and A. P. Hekstra. Perceptual evaluation of speech quality (pesq)-a new method for speech quality assessment of telephone networks and codecs. In *2001 IEEE International Conference on Acoustics, Speech, and Signal Processing. Proceedings (Cat. No.01CH37221)*, volume 2, pp. 749–752 vol.2, 2001. doi: 10.1109/ICASSP.2001.941023.

Jascha Sohl-Dickstein, Eric Weiss, Niru Maheswaranathan, and Surya Ganguli. Deep unsupervised learning using nonequilibrium thermodynamics. In *International Conference on Machine Learning*, pp. 2256–2265. PMLR, 2015.

Jiaming Song, Chenlin Meng, and Stefano Ermon. Denoising diffusion implicit models. *arXiv preprint arXiv:2010.02502*, 2020a.

Yang Song and Stefano Ermon. Generative modeling by estimating gradients of the data distribution. *arXiv preprint arXiv:1907.05600*, 2019.

Yang Song, Jascha Sohl-Dickstein, Diederik P Kingma, Abhishek Kumar, Stefano Ermon, and Ben Poole. Score-based generative modeling through stochastic differential equations. *arXiv preprint arXiv:2011.13456*, 2020b.

C. H. Taal, R. C. Hendriks, R. Heusdens, and J. Jensen. An algorithm for intelligibility prediction of time–frequency weighted noisy speech. *IEEE Transactions on Audio, Speech, and Language Processing*, 19(7):2125–2136, 2011. doi: 10.1109/TASL.2011.2114881.

Arash Vahdat and Jan Kautz. Nvae: A deep hierarchical variational autoencoder. *arXiv preprint arXiv:2007.03898*, 2020.

Ivan Vovk. Wavegrad. `https://github.com/ivanvovk/WaveGrad`, 2020.

Daniel Watson, Jonathan Ho, Mohammad Norouzi, and William Chan. Learning to efficiently sample from diffusion probabilistic models. *arXiv preprint arXiv:2106.03802*, 2021.

Fisher Yu, Yinda Zhang, Shuran Song, Ari Seff, and Jianxiong Xiao. Lsun: Construction of a large-scale image dataset using deep learning with humans in the loop. *arXiv preprint arXiv:1506.03365*, 2015.

A Proofs

A.1 Proof of lemma 1

Lemma 1. *Let $\theta_0 \in \mathbb{R}$, Assuming $\forall t \in \{1, ..., T\}$, $k_t = \dfrac{\beta_t}{\alpha_t {\theta_0}^2}$, $\theta_t = \sqrt{\bar{\alpha}_t}\theta_0$, and $g_t \sim \Gamma(k_t, \theta_t)$. Then $\forall t \in \{1, ..., T\}$ the following hold:*

$$E(g_t - E(g_t)) = 0, V(g_t - E(g_t)) = \beta_t \tag{12}$$

$$x_t = \sqrt{\bar{\alpha}_t} x_0 + (\bar{g}_t - E(\bar{g}_t)) \tag{13}$$

where $\bar{g}_t \sim \Gamma(\bar{k}_t, \theta_t)$ and $\bar{k}_t = \sum_{i=1}^{t} k_i$

Proof. The first part of Eq. 12 is immediate. The variance part is also straightforward:

$$V(g_t - E(g_t)) = k_t {\theta_t}^2 = \beta_t$$

Eq. 13 is proved by induction on $t \in \{1, ...T\}$. For $t = 1$:

$$x_1 = \sqrt{1-\beta_1}x_0 + g_1 - E(g_1)$$

since $\bar{k}_1 = k_1, \bar{g}_1 = g_1$. We also have that $\sqrt{1-\beta_1} = \sqrt{\bar{\alpha}_1}$. Thus we have:

$$x_1 = \sqrt{\bar{\alpha}_1}x_0 + (\bar{g}_1 - E(\bar{g}_1))$$

Assume Eq. 13 holds for some $t \in \{1, ...T\}$. The next iteration is obtained as

$$\begin{aligned} x_{t+1} &= \sqrt{1-\beta_{t+1}}x_t + g_{t+1} - E(g_{t+1}) && (22)\\ &= \sqrt{1-\beta_{t+1}}(\sqrt{\bar{\alpha}_t}x_0 + (\bar{g}_t - E(\bar{g}_t))) + g_{t+1} - E(g_{t+1}) && (23)\\ &= \sqrt{\bar{\alpha}_{t+1}}x_0 + \sqrt{1-\beta_{t+1}}\bar{g}_t + g_{t+1} - (\sqrt{1-\beta_{t+1}}E(\bar{g}_t) + E(g_{t+1})) && (24) \end{aligned}$$

It remains to be proven that (i) $\sqrt{1-\beta_{t+1}}\bar{g}_t + g_{t+1} = \bar{g}_{t+1}$ and (ii) $\sqrt{1-\beta_{t+1}}E(\bar{g}_t) + E(g_{t+1}) = E(\bar{g}_{t+1})$. Since $\bar{g}_t \sim \Gamma(\bar{k}_t, \theta_t)$ hold, then:

$$\sqrt{1-\beta_{t+1}}\bar{g}_t \sim \Gamma(\bar{k}_t, \sqrt{1-\beta_{t+1}}\theta_t) = \Gamma(\bar{k}_t, \theta_{t+1})$$

Therefore, we prove (i):

$$\sqrt{1-\beta_{t+1}}\bar{g}_t + g_{t+1} \sim \Gamma(\bar{k}_t + k_{t+1}, \theta_{t+1}) = \Gamma(\bar{k}_{t+1}, \theta_{t+1})$$

which implies that $\sqrt{1-\beta_{t+1}}\bar{g}_t + g_{t+1}$ and $\bar{g}_{t+1}$ have the same probability distribution.

Furthermore, by the linearity of the expectation, one can obtain (ii):

$$\begin{aligned} \sqrt{1-\beta_{t+1}}E(\bar{g}_t) + E(g_{t+1}) &= E(\sqrt{1-\beta_{t+1}}\bar{g}_t + g_{t+1})\\ &= E(\bar{g}_{t+1}) \end{aligned}$$

Thus, we have:

$$x_{t+1} = \sqrt{\bar{\alpha}_{t+1}}x_0 + (\bar{g}_{t+1} - E(\bar{g}_{t+1}))$$

which ends the proof by induction. □

A.2 Proof of Lemma 2

Lemma 2. *Denote $q(x_{t-1}|x_0, x_t)$ as the reverse process of the proposed Gamma diffusion model. Then, the reverse process is proportional to:*

$$q(x_{t-1}|x_0, x_t) \propto \frac{X_t^{k_t-1}e^{-X_t/\theta_t}\bar{X}_{t-1}^{\bar{k}_{t-1}-1}e^{-\bar{X}_{t-1}/\theta_{t-1}}}{\bar{X}_t^{\bar{k}_t-1}e^{-\bar{X}_t/\theta_t}} \tag{15}$$

where

1. $X_t = x_t - \sqrt{1-\beta_t}x_{t-1} + k_t\theta_t$
2. $\bar{X}_t = x_t - \sqrt{\bar{\alpha}_t}x_0 + \bar{k}_t\theta_t$
3. $\bar{X}_{t-1} = x_{t-1} - \sqrt{\bar{\alpha}_{t-1}}x_0 + \bar{k}_{t-1}\theta_{t-1}$

Proof. The reverse process is given by:

$$q(x_{t-1}|x_0, x_t) = q(x_t|x_{t-1}, x_0)\frac{q(x_{t-1}|x_0)}{q(x_t|x_0)} \tag{25}$$

Next, one can calculate each one of the three main components of the reverse process, i.e. (i) $q(x_t|x_{t-1}, x_0)$, (ii) $q(x_{t-1}|x_0)$ and (iii) $q(x_t|x_0)$. Since q is memoryless, $q(x_t|x_{t-1}, x_0) = q(x_t|x_{t-1})$. Therefore, the first component (i) of Eq. 25 is the forward process. The forward process is given by:

$$\begin{aligned} q(x_t|x_{t-1}) &= p(g_t = x_t - \sqrt{1-\beta_t}x_{t-1} + k_t\theta_t) && (26) \\ &= \frac{(x_t - \sqrt{1-\beta_t}x_{t-1} + k_t\theta_t)^{k_t-1} e^{-(x_t - \sqrt{1-\beta_t}x_{t-1} + k_t\theta_t)/\theta_t}}{\Gamma(k_t)\theta_t^{k_t}} && (27) \end{aligned}$$

The second component of Eq.25 is given by:

$$q(x_{t-1}|x_0) = \frac{(x_{t-1} - \sqrt{\bar{\alpha}_{t-1}}x_0 + \bar{k}_{t-1}\theta_{t-1})^{\bar{k}_{t-1}-1} e^{-(x_t - \sqrt{\bar{\alpha}_{t-1}}x_0 + \bar{k}_{t-1}\theta_{t-1})/\theta_{t-1}}}{\Gamma(\bar{k}_{t-1})\theta_t^{\bar{k}_{t-1}}} \tag{28}$$

Similarly, the third component of Eq.25 is given by:

$$q(x_t|x_0) = p(\bar{g}_t = x_t - \sqrt{\bar{\alpha}_t}x_0 + \bar{k}_t\theta_t) = \frac{(x_t - \sqrt{\bar{\alpha}_t}x_0 + \bar{k}_t\theta_t)^{\bar{k}_t-1} e^{-(x_t - \sqrt{\bar{\alpha}_t}x_0 + \bar{k}_t\theta_t)/\theta_t}}{\Gamma(\bar{k}_t)\theta_t^{\bar{k}_t}} \tag{29}$$

Overall, the reverse process $q(x_{t-1}|x_0, x_t)$ is given by:

$$\begin{aligned} q(x_{t-1}|x_0, x_t) = &\frac{\left((x_t - \sqrt{1-\beta_t}x_{t-1} + k_t\theta_t)^{k_t-1} e^{-(x_t - \sqrt{1-\beta_t}x_{t-1} + k_t\theta_t)/\theta_t}\right)}{\Gamma(k_t)\theta_t} \\ &\cdot \frac{\left((x_{t-1} - \sqrt{\bar{\alpha}_{t-1}}x_0 + \bar{k}_{t-1}\theta_{t-1})^{\bar{k}_{t-1}-1} e^{-(x_t - \sqrt{\bar{\alpha}_{t-1}}x_0 + \bar{k}_{t-1}\theta_{t-1})/\theta_{t-1}}\right)}{\Gamma(\bar{k}_{t-1})\theta_t^{\bar{k}_{t-1}}} \\ &\cdot \frac{\Gamma(\bar{k}_t)\theta_t^{\bar{k}_t}}{\left((x_t - \sqrt{\bar{\alpha}_t}x_0 + \bar{k}_t\theta_t)^{\bar{k}_t-1} e^{-(x_t - \sqrt{\bar{\alpha}_t}x_0 + \bar{k}_t\theta_t)/\theta_t}\right)} \end{aligned} \tag{30}$$

One can denote:

1. $X_t = x_t - \sqrt{1-\beta_t}x_{t-1} + k_t\theta_t$
2. $\bar{X}_t = x_t - \sqrt{\bar{\alpha}_t}x_0 + \bar{k}_t\theta_t$
3. $\bar{X}_{t-1} = x_{t-1} - \sqrt{\bar{\alpha}_{t-1}}x_0 + \bar{k}_{t-1}\theta_{t-1}$

Thus, the reverse process $q(x_{t-1}|x_0, x_t)$ is proportional to:

$$q(x_{t-1}|x_0, x_t) \propto \frac{X_t^{k_t-1} e^{-X_t/\theta_t} \bar{X}_{t-1}^{\bar{k}_{t-1}-1} e^{-\bar{X}_{t-1}/\theta_{t-1}}}{\bar{X}_t^{\bar{k}_t-1} e^{-\bar{X}_t/\theta_t}} \tag{31}$$

□

A.3 Proof of lemma 3

Lemma 3. *The L_{t-1} for the proposed Gamma diffusion model is upper bounded by the following L_1 norm:*

$$L_{t-1} \leq \left(C_1 + C_2 + \frac{C_3}{\bar{g}_t} + \frac{C_4}{\bar{g}_{t-1}}\right)|x_0 - \hat{x}_0| \tag{20}$$

where C_1, C_2, C_3 and C_4 are constant terms.

Proof. We can calculate the L_{t-1} with the exact form:

$$L_{t-1} = D_{KL}(q(x_{t-1}|x_0, x_t)||p_\theta(x_{t-1}|\hat{x}_0, x_t)) = E_{q(x_{t-1}|x_0,x_t)} \log\left(\frac{q(x_{t-1}|x_0, x_t)}{p_\theta(x_{t-1}|\hat{x}_0, x_t)}\right) \tag{32}$$

Using Eq.15 the RHS of Eq.32 become:

$$\log\left(\frac{q(x_{t-1}|x_0, x_t)}{p_\theta(x_{t-1}|\hat{x}_0, x_t)}\right) = (\bar{k}_{t-1} - 1)\log(\frac{\bar{X}_{t-1}}{\hat{X}_{t-1}}) - \frac{\bar{X}_{t-1} - \hat{X}_{t-1}}{\theta_{t-1}} - (\bar{k}_t - 1)\log(\frac{\bar{X}_t}{\hat{X}_t}) + \frac{\bar{X}_t - \hat{X}_t}{\theta_t} \tag{33}$$

One can show that the four terms present in the previous equation can be upper bounded with the L1 distance between the predicted $\hat{x}_0$ and the ground truth x_0:

- $|\frac{\bar{X}_{t-1}-\hat{X}_{t-1}}{\theta_{t-1}}| = |(x_0 - \hat{x}_0)\frac{\sqrt{\bar{\alpha}_{t-1}}}{\theta_{t-1}}| \leq C_1|x_0 - \hat{x}_0|$
- $|\frac{\bar{X}_t-\hat{X}_t}{\theta_t}| = |(x_0 - \hat{x}_0)\frac{\sqrt{\bar{\alpha}_t}}{\theta_t}| \leq C_2|x_0 - \hat{x}_0|$
- $(\bar{k}_t - 1)\log(\frac{\bar{X}_t}{\hat{X}_t}) = (\bar{k}_t - 1)\log\left(\frac{x_t - \sqrt{\bar{\alpha}_t}x_0 + \bar{k}_t\theta_t}{x_t - \sqrt{\bar{\alpha}_t}\hat{x}_0 + \bar{k}_t\theta_t}\right) = \log\left(1 + \frac{\sqrt{\bar{\alpha}_t}(x_0 - \hat{x}_0)}{x_t - \sqrt{\bar{\alpha}_t}\hat{x}_0 + \bar{k}_t\theta_t}\right) \leq |\frac{\sqrt{\bar{\alpha}_t}(x_0 - \hat{x}_0)}{x_t - \sqrt{\bar{\alpha}_t}\hat{x}_0 + \bar{k}_t\theta_t}| = \frac{C_3}{\bar{g}_t}|x_0 - \hat{x}_0|$
- $(\bar{k}_{t-1} - 1)\log(\frac{\bar{X}_{t-1}}{\hat{X}_{t-1}}) = \log\left(1 + \frac{\sqrt{\bar{\alpha}_{t-1}}(x_0 - \hat{x}_0)}{x_{t-1} - \sqrt{\bar{\alpha}_{t-1}}\hat{x}_0 + \bar{k}_{t-1}\theta_{t-1}}\right)$
  $\leq |\frac{\sqrt{\bar{\alpha}_{t-1}}(x_0 - \hat{x}_0)}{x_{t-1} - \sqrt{\bar{\alpha}_{t-1}}\hat{x}_0 + \bar{k}_{t-1}\theta_{t-1}}| = \frac{C_4}{\bar{g}_{t-1}}|x_0 - \hat{x}_0|$

The complete form of the L_{t-1} upper bound can be expressed as follows:

$$L_{t-1} \leq E_{q(x_{t-1}|x_0,x_t)}\left(C_1 + C_2 + \frac{C_3}{\bar{g}_t} + \frac{C_4}{\bar{g}_{t-1}}\right)|x_0 - \hat{x}_0| = \left(C_1 + C_2 + \frac{C_3}{\bar{g}_t} + \frac{C_4}{\bar{g}_{t-1}}\right)|x_0 - \hat{x}_0| \tag{34}$$

□

A.4 Proof of Lemma 4

Lemma 4. *Minimizing the variational lower bound for DDGM (i.e. L_t for $t \geq 1$) is equivalent to minimizing the L1 norm between the sampled noise and the estimated noise:*

$$\mathcal{L} = \left|\frac{\bar{g}_t - \bar{k}_t\theta_t}{\sqrt{1 - \bar{\alpha}_t}} - \varepsilon_\theta(x_t, t)\right| \tag{21}$$

Proof. From Eq.34, the variational lower bound of DDGM is given by $L_{t-1} \leq \left(C_1 + C_2 + \frac{C_3}{\bar{g}_t} + \frac{C_4}{\bar{g}_{t-1}}\right)|x_0 - \hat{x}_0|$. Substitute Eq.19 and Eq.11 to the variational lower bound we have:

$$L_{t-1} \leq \left(C_1 + C_2 + \frac{C_3}{\bar{g}_t} + \frac{C_4}{\bar{g}_{t-1}}\right) |x_0 - \hat{x}_0| \tag{35}$$

$$= \left(C_1 + C_2 + \frac{C_3}{\bar{g}_t} + \frac{C_4}{\bar{g}_{t-1}}\right) \left|x_0 - \frac{x_t - \sqrt{1-\bar{\alpha}_t}\varepsilon_\theta(x_t, t)}{\sqrt{\bar{\alpha}_t}}\right| \tag{36}$$

$$= \left(C_1 + C_2 + \frac{C_3}{\bar{g}_t} + \frac{C_4}{\bar{g}_{t-1}}\right) \frac{1}{\sqrt{\bar{\alpha}_t}} \left|\sqrt{\bar{\alpha}_t}x_0 - x_t + \sqrt{1-\bar{\alpha}_t}\varepsilon_\theta(x_t, t)\right| \tag{37}$$

$$= \left(C_1 + C_2 + \frac{C_3}{\bar{g}_t} + \frac{C_4}{\bar{g}_{t-1}}\right) \frac{1}{\sqrt{\bar{\alpha}_t}} \left|\sqrt{\bar{\alpha}_t}x_0 - \sqrt{\bar{\alpha}_t}x_0 - (\bar{g}_t - \bar{k}_t\theta_t) + \sqrt{1-\bar{\alpha}_t}\varepsilon_\theta(x_t, t)\right| \tag{38}$$

$$= \left(C_1 + C_2 + \frac{C_3}{\bar{g}_t} + \frac{C_4}{\bar{g}_{t-1}}\right) \frac{1}{\sqrt{\bar{\alpha}_t}} \left|(\bar{g}_t - \bar{k}_t\theta_t) - \sqrt{1-\bar{\alpha}_t}\varepsilon_\theta(x_t, t)\right| \tag{39}$$

$$= \left(C_1 + C_2 + \frac{C_3}{\bar{g}_t} + \frac{C_4}{\bar{g}_{t-1}}\right) \frac{\sqrt{1-\bar{\alpha}_t}}{\sqrt{\bar{\alpha}_t}} \left|\frac{\bar{g}_t - \bar{k}_t\theta_t}{\sqrt{1-\bar{\alpha}_t}} - \varepsilon_\theta(x_t, t)\right| \tag{40}$$

Since we are minimizing the variational lower bound, one can drop the constant term $\left(C_1 + C_2 + \frac{C_3}{\bar{g}_t} + \frac{C_4}{\bar{g}_{t-1}}\right) \frac{\sqrt{1-\bar{\alpha}_t}}{\sqrt{\bar{\alpha}_t}}$. Therefore, minimizing the variational lower bound is equal to minimizing the term $\left|\frac{\bar{g}_t - \bar{k}_t\theta_t}{\sqrt{1-\bar{\alpha}_t}} - \varepsilon_\theta(x_t, t)\right|$. □